Siberian Branch of Russian Academy of Science

BUDKER INSTITUTE OF NUCLEAR PHYSICS

M.N. Achasov, A.V. Berdyugin, A.V. Bozhenok, D.A. Bukin, S.V. Burdin,
T.V. Dimova, V.P. Druzhinin , M.S. Dubrovin, I.A. Gaponenko, V.B. Golubev,
V.N. Ivanchenko, A.A. Korol, S.V. Koshuba, E.V. Pakhtusova, A.A. Salnikov,
S.I. Serednyakov, V.V. Shary, Yu.M. Shatunov, V.A. Sidorov, Z.K. Silagadze

EXPERIMENTAL STUDY OF THE PROCESSES $e^+e^- \to \phi \to \eta\gamma$, $\pi^0\gamma$ AT VEPP-2M

Budker INP 99-39

NOVOSIBIRSK
1999

Experimental study of the processes $e^+e^- \to \phi \to \eta\gamma,\ \pi^0\gamma$ at VEPP-2M

M.N. Achasov, A.V. Berdyugin, A.V. Bozhenok, D.A. Bukin, S.V. Burdin, T.V. Dimova, V.P. Druzhinin, M.S. Dubrovin, I.A. Gaponenko, V.B. Golubev, V.N. Ivanchenko, A.A. Korol, S.V. Koshuba, E.V. Pakhtusova, A.A. Salnikov, S.I. Serednyakov, V.V. Shary, Yu.M. Shatunov, V.A. Sidorov, Z.K. Silagadze

Budker Institute of Nuclear Physics SB RAS
630090 Novosibirsk, Russia

Abstract

The processes $e^+e^- \to \eta\gamma,\ \pi^0\gamma \to 3\gamma$ were studied in the SND experiment at the VEPP-2M collider in the energy region of ϕ-meson. The branching ratios obtained in this study are $\mathrm{Br}(\phi \to \eta\gamma) = (1.338 \pm 0.012 \pm 0.052)\%$ and $\mathrm{Br}(\phi \to \pi^0\gamma) = (1.226 \pm 0.036^{+0.096}_{-0.089}) \times 10^{-3}$. A comparison of the experimental data with the different theoretical models was performed.

1 Introduction

The studies of the radiative decays of light vector mesons (ρ, ω, ϕ) in e^+e^- collisions play an important role in understanding of the electromagnetic structure of $q\overline{q}$-states and low-energy behavior of strong interactions [1]. Theoretical models employed here describe radiative decays of mesons [2, 3, 4] and the hadronization processes in e^+e^- collisions [5, 6]. Unfortunately the statistics collected on e^+e^-colliders in the low energy region presently does not allow unambiguous determination of the parameters of these models or discrimination between different models. With the beginning of CMD-2 [7] and SND [8] experiments at the VEPP-2M collider, a new opportunity emerges to increase significantly experimental statistics and reduce the uncertainties of the observed results.

In this work we present the results of studies of the processes $e^+e^- \to \eta\gamma$, $\pi^0\gamma$ in the three-photon final state in the ϕ-meson region, which were obtained with the experimental data gathered in the SND experiment. Previous information on these processes is mainly from the ND [9], CMD-2 [10], and SND [11] measurements. Section 2 gives a brief description of the apparatus and the experimental conditions, section 3 describes the data analysis procedure, section 4 gives the results obtained for the different theoretical models, and section 5 discusses briefly the obtained results.

2 Apparatus and experimental conditions

SND is a general-purpose non-magnetic detector (Fig. 1). More detailed description of the detector can be found in the ref. [8]. SND was designed and optimized for the observation of neutral particles. The main part of the detector is an electromagnetic calorimeter built of 1632 NaI(Tl) crystals. Full thickness of the calorimeter for the particles originating from the interaction point is $13.5X_0$. The calorimeter provides a good energy resolution for photons (Fig. 2), which can be approximated as $\sigma_E(E)/E = 4.2\%/E(GeV)^{1/4}$ [12]. An angular resolution is determined primarily by the size of the crystals and is approximately equal to $\sigma_{\theta,\varphi} = 1.5^\circ$ [13]. The calorimeter and the event reconstruction program allow to detect photons with the energies above 20 MeV with a solid angle coverage 90% of 4π.

The experiments with the SND detector were carried out at the VEPP-2M collider with the average luminosity $\sim 10^{30}$ cm^{-2}sec^{-2}. In this work we present the results based on the experimental statistics collected during 1996 year, which includes 7 scans of the energy region 985–1040 MeV. Total integrated luminosity accumulated in these scans is 4.3 pb^{-1}, corresponding to approximately 8.2×10^6 events of ϕ meson decays.

3 Data analysis

In this work two radiative decays of ϕ-meson were studied in the following processes:

$$e^+e^- \to \eta\gamma \to \gamma\gamma\gamma, \tag{1}$$

$$e^+e^- \to \pi^0\gamma \to \gamma\gamma\gamma. \tag{2}$$

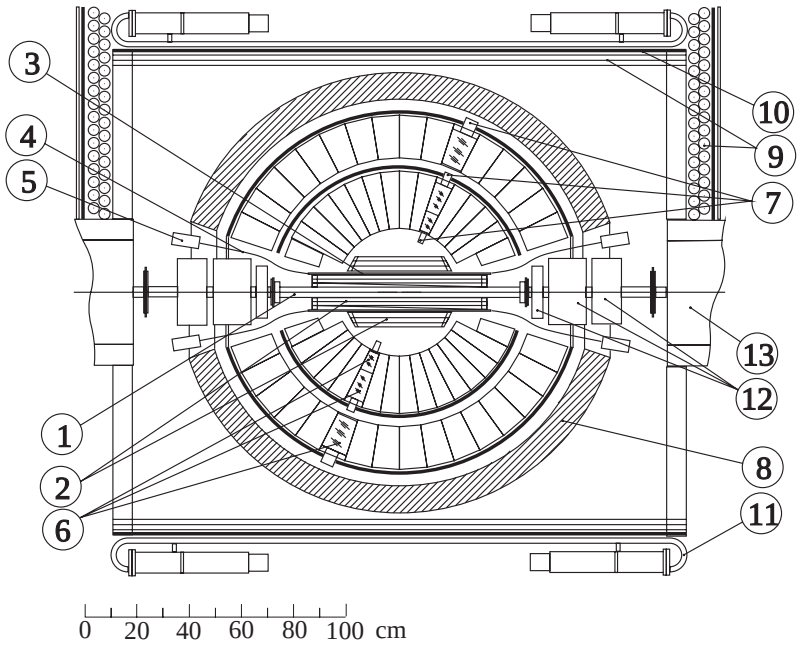

Figure 1: SND detector, cut along the beams; 1 — beam pipe, 2 — drift chambers, 3 — scintillation counters, 4 — light guides, 5 — PMTs, 6 — NaI(Tl) crystals, 7 — vacuum phototriodes, 8 — iron absorber, 9 — streamer tubes, 10 — 1cm iron plates, 11 — scintillation counters, 12 and 13 — elements of collider magnetic system.

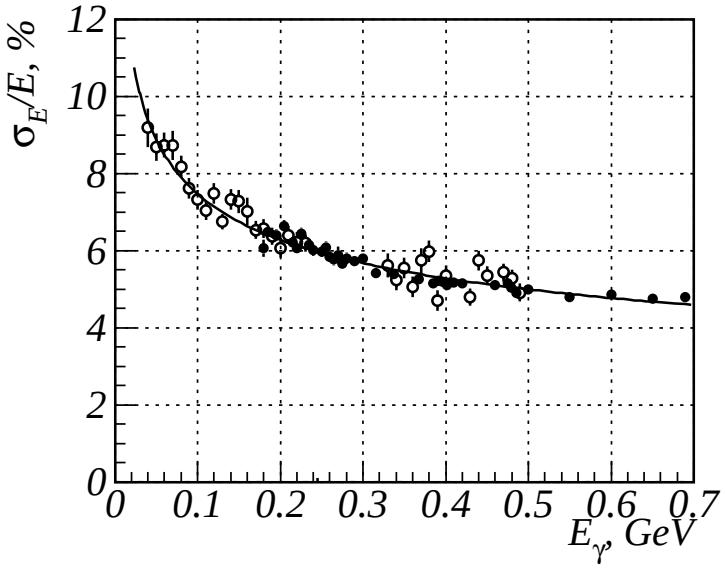

Figure 2: Energy dependence of the calorimeter energy resolution. The data were obtained from $e^+e^- \to \gamma\gamma$ (dots) and $e^+e^- \to e^+e^-\gamma$ (open circles) processes.

with the main background coming from non-resonant QED three-quanta annihilation:

$$e^+e^- \to \gamma\gamma\gamma \,(\mathrm{QED}) \tag{3}$$

For studies of cross-sections of the investigated processes near the resonance maximum a procedure was developed for the selection of events with three detected photons. For the suppression of spurious signals in the calorimeter, which appear mainly in the crystals closest to the beam, additional restrictions were imposed on the energies and angles of the reconstructed photons. These restrictions were based on the detailed study of $e^+e^- \to \gamma\gamma$ events. Preliminary selection included following conditions:

1. presence of three or four reconstructed photons,
2. total energy deposition in the calorimeter (E_{tot}) is in the range from $0.7\sqrt{s}$ to $1.2\sqrt{s}$, where $s = 4E^2_{\mathrm{beam}}$,
3. sum of the momenta of all particles is lower than $0.2E_{\mathrm{tot}}/c$,
4. minimal energy of the photons is 50 MeV; polar angle for the photons with energies 50–100 MeV is in the range $45^\circ < \theta < 135^\circ$, for the photons with the energies higher than 100 MeV — $27^\circ < \theta < 153^\circ$.

The number of events, which passed this preliminary selection, was about 139 000. Further selection was based on the kinematic fit of the events. Employing the 4-momentum conservation it is possible with this procedure to build statistical tests for the different intermediate states in the observed event. For each event the following four hypotheses were tested:

1. hypothesis $H_{2\gamma}$: two most energetic photons are due to the process $e^+e^- \to \gamma\gamma$. This hypothesis was used for the further suppression of spurious signals in the calorimeter,
2. hypothesis $H_{3\gamma}$: three photons in the event are from the process (3),
3. hypothesis $H_{\eta\gamma}$: three photons in the event are from the process (1),
4. hypothesis $H_{\pi\gamma}$: three photons in the event are from the process (2).

One can notice that the hypotheses $H_{\eta\gamma}$ and $H_{\pi\gamma}$ are similar to the hypothesis $H_{3\gamma}$, but with the additional constraint on the invariant mass of the pair of photons. The performance of the kinematic fit procedure can be seen in Fig. 3, where the invariant mass spectra of all photon pairs are plotted, before and after the kinematic fit with the hypothesis $H_{3\gamma}$. A significant improvement of the resolution is clearly seen, especially for the η-meson mass.

For each of the above hypotheses a test statistics was built: $\xi_i = \mathrm{Prob}(\chi^2_i)$, where χ^2_i is the χ^2 value obtained in the kinematic fit under hypothesis H_i. For the correctly selected hypothesis the distribution of the corresponding statistics ξ_i is close to uniform. Using these statistics the events which satisfy $H_{3\gamma}$ hypothesis ($\xi_{3\gamma} > 0.003$) but do not satisfy $H_{2\gamma}$ hypothesis ($\xi_{2\gamma} < 0.0005$) were selected. These events were divided further into 4 non-overlapping classes using the statistics $\xi_{\eta\gamma}$ and $\xi_{\pi\gamma}$:

A. class containing mainly the events of the processes (1) and (3) ($\xi_{\eta\gamma} > \alpha$ and $\xi_{\pi\gamma} < \beta$),

B. class containing mainly the events of the processes (2) and (3) ($\xi_{\pi\gamma} > \alpha$ and $\xi_{\eta\gamma} < \beta$),

C. class containing the events of all three processes ($\xi_{\pi\gamma} > \beta$ and $\xi_{\eta\gamma} > \beta$),

D. class containing mainly the events of the process (3) ($\xi_{\pi\gamma} < \beta$ and $\xi_{\eta\gamma} < \beta$),

where the parameters $\alpha = 0.05$ and $\beta = 0.0003$ define the size of the critical regions for the hypotheses $H_{\eta\gamma}$ and $H_{\pi\gamma}$. The number of thus selected events in each class is given in the table 1.

Tables 2–4 display the summary data for the above selection procedure. To reduce the size of theses tables, the data points from different scans with the close energies were merged together. Table 2 shows these combined data points, giving for each point a c.m. energy range and an

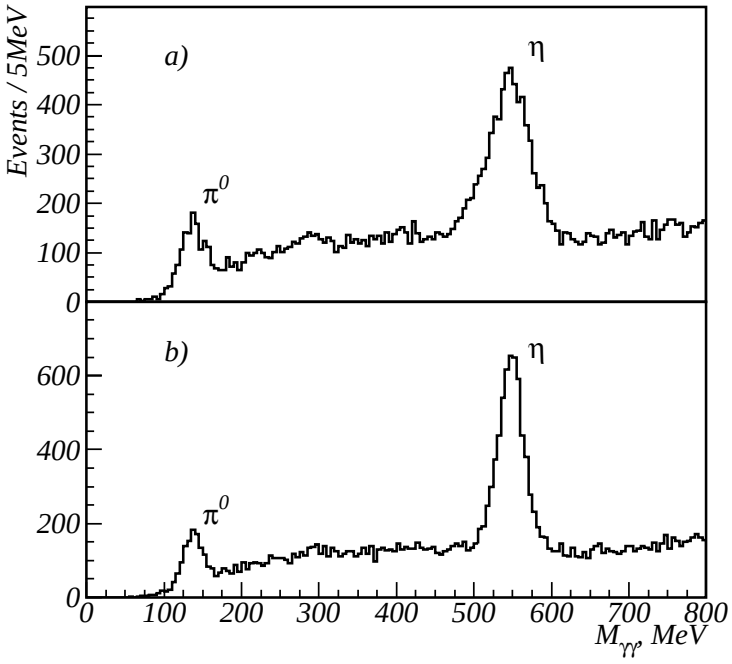

Figure 3: Comparison of spectra of the invariant masses of photon pairs in 3γ events before (plot a) and after (plot b) the $H_{3\gamma}$ kinematic fit. Spectra include three entries per event.

Table 1: Number of events in each of the selection classes, and selection efficiencies in the ϕ resonance maximum.

Selection class	A	B	C	D
Total events	20 356	2 224	2 821	7 376
Process	Efficiency, %			
(1)	44.	0.02	2.4	0.3
(2)	0.1	14.	11.	0.3
(3)	1.2	0.31	0.31	4.1

Table 2: Experimental data points. Each entry contains the experimental point number, energy range for this point, and the integrated luminosity.

Point	Energy, MeV	Lumin., 1/nb
1	985.13 – 986.04	195.1 ± 1.0
2	1004.51 – 1005.41	193.6 ± 1.0
3	1010.34 – 1011.19	248.8 ± 1.2
4	1015.62 – 1016.52	287.9 ± 1.2
5	1016.98 – 1017.34	239.0 ± 1.1
6	1017.94 – 1018.48	393.5 ± 1.4
7	1018.84 – 1019.43	1223.7 ± 2.4
8	1019.74 – 1020.39	489.4 ± 1.6
9	1020.72 – 1021.33	321.7 ± 1.4
10	1021.69 – 1021.95	184.6 ± 1.0
11	1022.14 – 1022.79	149.5 ± 0.9
12	1027.64 – 1028.59	198.7 ± 1.1
13	1033.38 – 1034.35	154.4 ± 0.9
14	1039.01 – 1039.30	23.9 ± 0.4
Total:		4303.8

integrated luminosity. Tables 3 and 4 show the data for the selection classes A and B respectively. For each energy point these tables display the number of the selected events, the selection efficiencies for the processes (1) or (2), value of the factor β_p (see eq. (4) below) for each process, the expected number of events for the process (3), the resulting value of the cross-section, and its error. We have to note here that the values of the cross-sections in the tables are given for the reference only, our further analysis did not use them. Instead, the initial data were used.

4 Cross-section determination

For the determination of the parameters of the processes (1) and (2), the energy dependence of the observed number of events in each of four selection classes was approximated by the following dependence

$$N_q^{th}(E) = L(E) \times \sum_p \sigma_p(E)\beta_p(E)\varepsilon_{q,p}(E), \tag{4}$$

where $N_q^{th}(E)$ is the expected number of events in the selection class q, $L(E)$ is the integrated luminosity in the energy point, $\sigma_p(E)$ is a cross-section of the process p, $\beta_p(E)$ is a factor taking into account radiative corrections [14] and a beam energy spread, $\varepsilon_{q,p}(E)$ is an efficiency of the selection algorithm for the process p in the selection class q. Summation is performed over the three main processes — (1), (2) and (3), a contribution from other processes, both resonant and non-resonant, estimated from the full simulation, is negligible.

The integrated luminosity $L(E)$ was estimated from the number of events of two-photon annihilation at large angles ($27^\circ < \theta < 163^\circ$). The statistical uncertainty of estimations is lower than 1% for most experimental points, systematic effects give an additional error of 2.5%.

For the description of the cross-section of processes $e^+e^- \to P\gamma$, where P is a pseudoscalar meson, the following dependence was used:

$$\sigma(s) = \frac{4\pi\alpha^2 F(s)}{s^{3/2}} \left| B_P + \mathrm{i} \sum_{V=\rho,\omega,\phi} \frac{g_{VP\gamma}}{g_V} \frac{m_V^2 e^{\mathrm{i}\varphi_V}}{D_V(s)} \right|^2, \tag{5}$$

where $F(s) = \left[(s - m_P^2)/2\sqrt{s}\right]^3$, and $D_V(s) = m_V^2 - s - \mathrm{i}\sqrt{s}\Gamma_V(s)$. An amplitude B_P describes a contribution from non-resonant intermediate states, its value is fixed by specific models as described below. Coupling constants $g_{VP\gamma}$ and g_V are related to the decay widths of vector meson $\Gamma(V \to P\gamma) = g_{VP\gamma}^2 F(m_V^2)/12\pi$ and $\Gamma(V \to e^+e^-) = 4\pi\alpha^2 m_V/g_V^2$. The contribution of the excited states, such as ρ' or ρ'', is expected to be small, and was not included in (5).

Table 3: Summary table of the data for the selection class A. Each entry in the table contains the experimental point number, number of selected events, efficiency of the selection for the process (1), factor β from eq. (4) for this process, expected number of the events for process (3), and the resulting cross-section of process $e^+e^- \to \eta\gamma$. Numbering of the energy points corresponds to the table 2.

Point	Events	Eff., %	β	N QED	$\sigma_{e^+e^-\to\eta\gamma}$, nb
1	98	39.7 ± 0.8	0.913	92.6	0.19 ± 0.50
2	98	43.4 ± 0.3	0.821	91.2	1.55 ± 0.55
3	226	43.7 ± 0.3	0.783	116.8	3.27 ± 0.56
4	893	43.9 ± 0.2	0.740	135.7	20.66 ± 0.89
5	1069	43.3 ± 0.2	0.729	110.8	32.43 ± 1.18
6	2351	43.5 ± 0.2	0.720	183.8	44.79 ± 1.08
7	9102	43.8 ± 0.2	0.729	577.1	55.59 ± 0.70
8	3369	43.4 ± 0.2	0.775	228.4	48.65 ± 0.97
9	1575	43.3 ± 0.2	0.854	149.9	30.55 ± 0.91
10	714	43.0 ± 0.2	0.930	85.4	21.72 ± 0.99
11	464	43.5 ± 0.2	1.000	70.1	15.47 ± 0.91
12	222	42.4 ± 0.3	1.659	92.0	2.37 ± 0.32
13	124	41.5 ± 0.5	2.636	71.5	0.79 ± 0.21
14	16	39.6 ± 0.7	3.978	10.9	0.35 ± 0.35
Total:	20356			2016.3	

Table 4: Summary table of the data for the selection class B. Each entry in the table contains the experimental point number, number of selected events, efficiency of the selection for the process (2), factor β from eq. (4) for this process, expected number of the events for process (3), and the resulting cross-section of process $e^+e^- \to \pi^0\gamma$. Numbering of the energy points corresponds to the table 2.

Point	Events	Eff., %	β	N QED	$\sigma_{e^+e^-\to\pi^0\gamma}$, nb
1	39	6.7 ± 0.2	2.292	31.2	0.26 ± 0.28
2	37	8.5 ± 0.2	1.650	27.0	0.37 ± 0.30
3	70	10.0 ± 0.2	1.299	33.2	1.15 ± 0.32
4	135	12.6 ± 0.2	0.916	37.1	2.97 ± 0.40
5	103	13.3 ± 0.2	0.864	30.4	2.68 ± 0.64
6	276	13.7 ± 0.2	0.825	49.9	5.16 ± 0.42
7	920	14.1 ± 0.2	0.834	154.1	5.40 ± 0.25
8	346	13.3 ± 0.2	0.919	61.0	4.81 ± 0.35
9	133	12.7 ± 0.2	1.116	39.8	2.07 ± 0.29
10	68	11.7 ± 0.2	1.374	22.6	1.54 ± 0.33
11	48	11.3 ± 0.2	1.663	18.4	1.07 ± 0.29
12	29	7.0 ± 0.2	16.38	23.2	0.03 ± 0.03
13	19	4.9 ± 0.1	126.4	17.3	0.00 ± 0.01
14	1	4.1 ± 0.2	37.18	2.5	-0.04 ± 0.05
Total:	2224			547.9	

Energy dependence of the full widths of vector mesons was determined from the sum of the widths of principal decay modes, as in [6]. Particularly, the energy dependence of the ρ-meson width was taken as

$$\Gamma_\rho(s) = \Gamma_\rho(m_\rho^2)\frac{F(s)}{F(m_\rho^2)}\frac{m_\rho^2}{s}. \tag{6}$$

The cross section of the process $e^+e^- \to V \to P\gamma$ in the resonance maximum is given by

$$\sigma_{VP\gamma} = \frac{12\pi\Gamma_{V\to e^+e^-}\Gamma_{V\to P\gamma}}{m_V^2\Gamma_V^2}. \tag{7}$$

Using this relation and (5), the cross section of the process $e^+e^- \to P\gamma$ can be rewritten as

$$\sigma(s) = \frac{F(s)}{s^{3/2}}\left|\sqrt{4\pi\alpha^2}B_P + \mathrm{i}\sum_{V=\rho,\omega,\phi} A_V\right|^2, \tag{8}$$

$$A_V = \sqrt{\sigma_{VP\gamma}\frac{m_V^3}{F(m_V^2)}}\frac{m_V\Gamma_V e^{\mathrm{i}\varphi_V}}{D_V(s)}. \tag{9}$$

The cross sections of the processes $e^+e^- \to P\gamma \to \gamma\gamma\gamma$, which participate in fitting of the experimental data with the eq. (4), include also the probability of the decay $P \to \gamma\gamma$, $\sigma_p(s) = \sigma(s)\times$ Br$(P \to \gamma\gamma)$. The numbers obtained from fitting of experimental data with the dependency (4) are the the values of the cross sections of processes $e^+e^- \to \phi \to P\gamma \to \gamma\gamma\gamma$ in the resonance maximum

$$\sigma_{\phi P} \equiv \sigma_{\phi P\gamma} \times \mathrm{Br}(P \to \gamma\gamma), \tag{10}$$

the parameters of ρ and ω mesons were fixed. As these values are obtained directly from the data, their errors include only the experimental uncertainties, and the model dependence.

The selection efficiency for the processes (1) and (2) in each selection class was determined from the Monte-Carlo simulation [15]. To reproduce an energy dependence of the efficiencies the simulation was performed in the whole energy region of the experiment, taking into account the radiative corrections. For the process (1) the energy dependence of the efficiency is rather weak and, to the desired precision, can be approximated by parabolic curve. For the process (2) the dependence is stronger and more complex, determined by larger radiative corrections. For this process a simulation was performed with the more detailed scan of the energy region, with the further use of a linear approximation between the simulated energy points. The values for the efficiencies for each process in the resonance maximum are presented in the table 1.

The cross section of the process (3) was described using the formulae from ref. [16], which do not take into account the radiative corrections. The efficiencies for this process were determined from the full simulation with the minimal energy of emitted photons 10 MeV and polar angles $18^\circ < \theta < 162^\circ$. The efficiency obtained from Monte-Carlo should be adjusted to take into account the influence of radiative corrections. For this, the factor β_p (eq. (4)) for this process, which now includes both the radiative corrections and efficiency adjustment, was determined from the fit of the experimental data of the selection class D. The value obtained in this way is $\beta = 0.96 \pm 0.01$. The resulting cross section fits well to the experimental data of the class D, thus allowing to fix the level of the cross section of the process (3) in all other selection classes. The uncertainty of the factor β_p determined in this way does not influence the final results due to the relatively small contribution of this process to the selection classes A and B.

Fit of the eq. (4) to the experimental data was performed using maximum likelyhood method. A likelyhood of the observation was described by modified Poisson probability function, which takes into account the uncertainty of the mean value of the expected number of events.

To estimate the model dependence of the obtained results the fit of the experimental data was performed for the different theoretical models, described in the following sections.

4.1 Vector dominance model

In the vector dominance model (VDM) the cross section of the processes $e^+e^- \to P\gamma$ is determined only by the number of poles identified with the vector mesons [2, 3], hence for VDM $B_P \equiv 0$. This is

the most common model used for the description of the cross sections in practically all experiments with the e^+e^- colliding beams at low energies ($2E < 1\,\mathrm{GeV}$).

Fitting of the observed number of events was performed simultaneously for the three selection classes, A, B, and C, the parameters determined from the fit were $\sigma_{\phi\eta}$ and $\sigma_{\phi\pi}$. For the masses and widths of all mesons their table values were used [17]. A consistent treatment of the model dependencies requires the determination of all parameters in the same model. Following this approach the widths of the decays $\rho,\omega \to \eta\gamma$ and $\rho,\omega \to \pi^0\gamma$ were taken from the ND analysis [9], which was performed also using VDM.

In the case $B_P = 0$ there exists an uncertainty in the definition of the phases of vector mesons φ_V, thus the phase of ρ meson was fixed at $\varphi_\rho = 0$. The value of the ω meson phase φ_ω was taken equal to φ_ρ, according to the quark model prediction. The value of the ϕ meson phase in the process (1) was set to $\varphi_\phi = 180^\circ$. During the analysis of the data a strong dependence was observed of the obtained cross section $\sigma_{\phi\pi}$ on the phase value φ_ϕ in the process (2). An exact and independent determination of the phase $\varphi_\phi(\pi\gamma)$ from the same statistics is impossible. Fit was performed with a value $\varphi_\phi(\pi\gamma) = (158 \pm 11)^\circ$, which was obtained by combination of the ND [9] and CMD-2 [18] measurements of this phase in the processes $e^+e^- \to \omega,\phi \to 3\pi$. The uncertainty of the phase was accounted for using the constrained fit technique.

As a result of the fit the following values of the cross section were obtained:

$$\sigma_{\phi\eta} = (22.16 \pm 0.20 \pm 0.59)\,\mathrm{nb}, \tag{11}$$

$$\sigma_{\phi\pi} = (5.12 \pm 0.15^{+0.38}_{-0.35})\,\mathrm{nb}. \tag{12}$$

In the quoted errors the first represent a statistical error, and the second – systematic. The main contributors to the systematic errors are uncertainties in the integrated luminosity (2.5%), and in the efficiency evaluation — 1% for the process (1), and 2% for the process (2). For the process (2) the uncertainty in the phase φ_ϕ was also included in the systematic error.

Using the table values of the decay probabilities [17]

$$\mathrm{Br}(\eta \to \gamma\gamma) = (39.21 \pm 0.34)\%, \tag{13}$$

$$\mathrm{Br}(\pi \to \gamma\gamma) = (98.798 \pm 0.0032)\%, \tag{14}$$

$$\mathrm{Br}(\phi \to e^+e^-) = (2.99 \pm 0.08) \times 10^{-4} \tag{15}$$

from (11,12) the relative widths of the decays were obtained, which are given in the part I of table 5 together with the χ^2 value obtained in the fit. Fig. 4 represents the visible cross section, $\sigma_{\mathrm{vis}} = N/L$, in two selection classes for all experimental points together with the theoretical curves obtained from the fit.

For a comparison, fitting of the experimental data was performed also with the fixed value of the phase $\varphi_\phi(\pi\gamma) = 180^\circ$. The result, displayed in the part II of table 5, reveals a strong dependence of the decay width $\phi \to \pi^0\gamma$ on the exact value of this phase. The fit quality, measured by the χ^2 value, in this case practically does not change.

4.2 Anomalous contribution

The next model discussed here is an extension of the VDM, and includes, in addition to the vector mesons-mediated diagrams, the contribution from the loop diagrams (anomalies). In this case B_P in (5) determines the value of the anomalous contribution [5], and is related to the two-photon width of the pseudoscalar meson $\Gamma_{P\to\gamma\gamma}$:

$$B_P = -\sqrt{\frac{16}{3\alpha}\frac{\Gamma_{P\to\gamma\gamma}}{m_P^3}}. \tag{16}$$

The value of this term is comparable in the magnitude with the contribution of ρ and ω mesons in the resonance region. It is worth mentioning here that the phase of B_P is fixed, thus allowing the determination of the absolute value of phases φ_V for all three vector mesons.

Fitting of the data was performed with the (5) using the above expression for B_P. Free parameters in this fit were $\sigma_{\phi\eta}$, $\sigma_{\phi\pi}$, $\varphi_\rho(\eta\gamma)$, $\varphi_\rho(\pi\gamma)$ and $\varphi_\phi(\pi\gamma)$. All other phases were fixed according to predictions of quark model: $\varphi_\omega(\eta\gamma) = \varphi_\rho(\eta\gamma)$, $\varphi_\phi(\eta\gamma) = \varphi_\rho(\eta\gamma) + 180^\circ$, $\varphi_\omega(\pi\gamma) =$

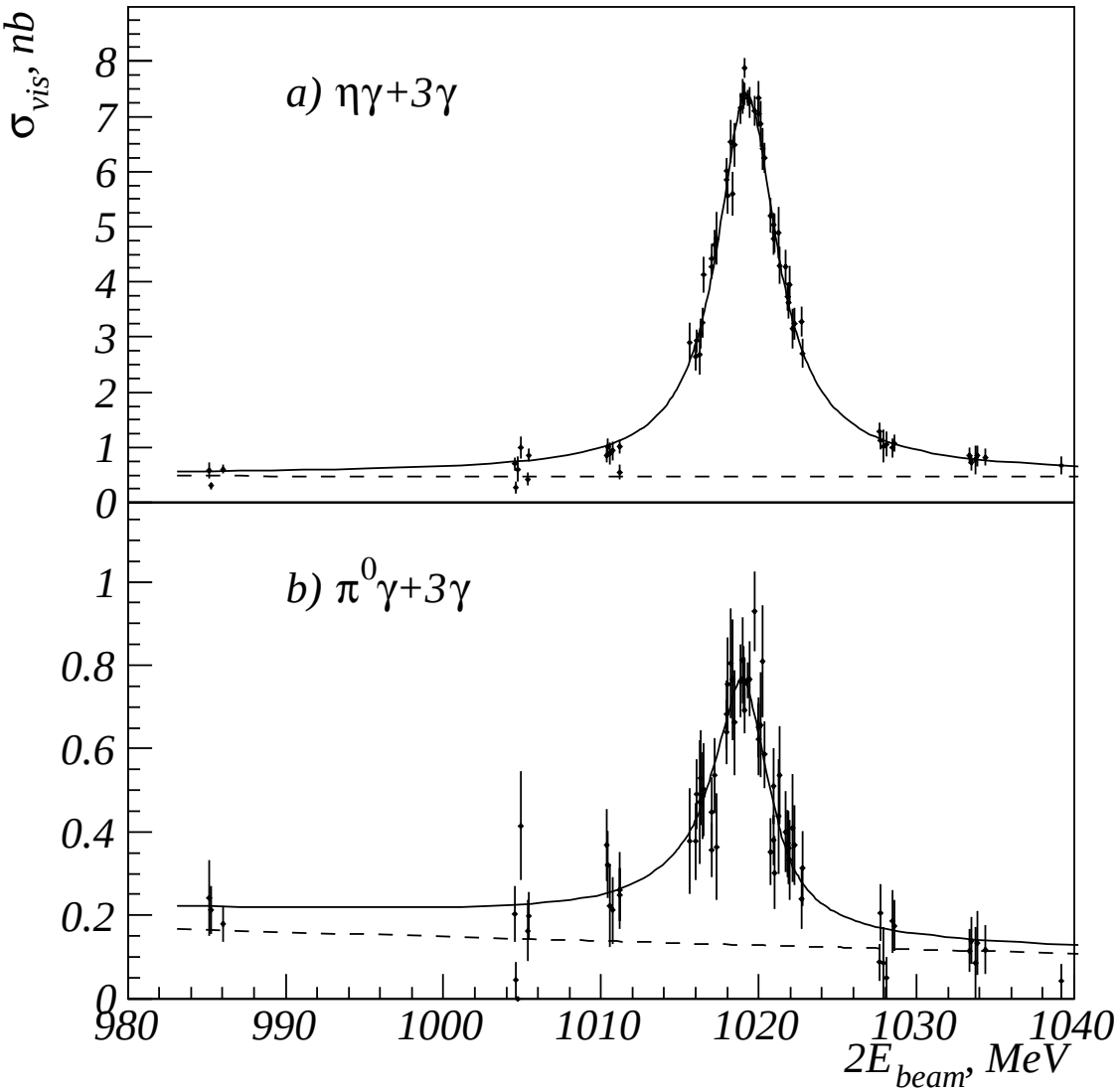

Figure 4: Visible cross-section for the selection classes A (plot a) and B (plot b). Curves are VDM fit. Dashed lines give the level of QED cross section.

Table 5: Measured cross-sections and branching ratios for the different models. Only statistical errors are quoted in this table.

P	η	π^0
(I) VDM, $\varphi_\phi(\pi\gamma) = 158^\circ$		
$\sigma_{\phi P}$, nb	22.16 ± 0.20	5.12 ± 0.15
$\mathrm{Br}(\phi \to P\gamma)$	$(1.338 \pm 0.012)\%$	$(1.226 \pm 0.036) \times 10^{-3}$
χ^2/DOF	212.4/211	
(II) VDM, $\varphi_\phi(\pi\gamma) = 180^\circ$		
$\sigma_{\phi P}$, nb	22.16 ± 0.20	5.82 ± 0.16
$\mathrm{Br}(\phi \to P\gamma)$	$(1.338 \pm 0.012)\%$	$(1.396 \pm 0.036) \times 10^{-3}$
χ^2/DOF	212.5/211	
(III) Anomalous contribution		
$\sigma_{\phi P}$, nb	23.16 ± 0.20	$5.39^{+1.12}_{-1.07}$
$\mathrm{Br}(\phi \to P\gamma)$	$(1.398 \pm 0.012)\%$	$(1.29^{+0.27}_{-0.26}) \times 10^{-3}$
$\varphi_\rho = \varphi_\omega$	$(10 \pm 14)^\circ$	$(52^{+11}_{-16})^\circ$
φ_ϕ	$\varphi_\rho + 180^\circ$	$(165^{+29}_{-39})^\circ$
χ^2/DOF	210.7/208	
(IV) Model-independent		
$\sigma_{\phi P}$, nb	21.7 ± 1.3	$5.82^{+0.27}_{-0.82}$
$\mathrm{Br}(\phi \to P\gamma)$	$(1.31 \pm 0.08)\%$	$(1.39^{+0.06}_{-0.20}) \times 10^{-3}$
$\mathrm{Re}A$, nb$^{1/2}$	-0.74 ± 0.18	$-0.78^{+0.08}_{-0.16}$
$\mathrm{Im}A$, nb$^{1/2}$	0.18 ± 0.81	$0.32^{+0.09}_{-0.32}$
χ^2/DOF	212.0/207	

$\varphi_\rho(\pi\gamma)$. For the consistency reasons, mentioned already in the previous section, the widths of the decays $\rho,\omega \to \eta\gamma$ and $\rho,\omega \to \pi^0\gamma$ were taken from work [5]. The set of the parameters obtained as the result of the fit is displayed in the part III of table 5. Resulting cross sections differ from the values obtained for VDM, the fact is more noticeable for the $\phi \to \eta\gamma$ decay. For the $\phi \to \pi^0\gamma$ decay the obtained cross section is somewhat intermediate case between two VDM fits discussed above, but in this case the observed uncertainty in the cross section is larger than in the VDM case, this fact is determined by the total uncertainty in the ϕ meson phase and the strong correlation between these two values.

The values for the phases of vector mesons obtained for this model differ from those obtained in ref. [5]. An additional fit was performed with the set of fixed phases obtained in [5]. A strong worsening of the fit quality was observed, the value of χ^2 in this case is equal to 260 for 211 degrees of freedom, which indicates rather low likelyhood for the observed data in this variant. The discrepancy observed for the phases can, possibly, be attributed to the different parameterization of the ρ shape used in [5], although we did not perform an exact analysis of its origin.

4.3 Model-independent check

An alternative approach to the parameterization of the cross section is based on the assumption about the near constant value of the non-resonant term of the amplitude, which includes pure non-resonant processes and also the tails of the ρ, ω mesons and possible higher states. This assumption should have a rather good precision in the energy region under study, which is quite narrow and remote from other resonances. Under this assumption the cross section of the process $e^+e^- \to P\gamma$ can be written as

$$\sigma_{e^+e^-\to P\gamma}(s) = \frac{F(s)}{s^{3/2}} \left|A_P - A_\phi\right|^2, \tag{17}$$

where the energy-independent term A_P determines the contribution of all intermediate mechanisms except $e^+e^- \to \phi \to P\gamma$, and A_ϕ is defined in (9). In this approach the parameters determined from the fit are $\sigma_{\phi\eta}$, $\sigma_{\phi\pi}$, and a complex amplitude A_P for each of the processes under study.

The set of the parameters obtained from the fit is displayed in the part IV of the table 5. As in the previous case, large uncertainties in the cross section values are observed, which come from

Table 6: Values of the non-resonant amplitude in the resonance maximum for different models. Errors given for the model-independent analysis (IV) are statistical only. Models (I-II) should have significantly smaller errors, for the model (III) the errors are the same or smaller than for model-independent analysis (IV).

$P\gamma$	$\eta\gamma$	$\pi^0\gamma$
(I) VDM, $\varphi_\phi(\pi\gamma) = 158^\circ$		
A, nb$^{1/2}$	$-0.99 + \mathrm{i}\,0.49$	$-0.91 + \mathrm{i}\,0.03$
(II) VDM, $\varphi_\phi(\pi\gamma) = 180^\circ$		
A, nb$^{1/2}$	$-0.99 + \mathrm{i}\,0.49$	$-0.82 + \mathrm{i}\,0.41$
(III) Anomaly contribution		
A, nb$^{1/2}(\rho+\omega)$	$-0.70 + \mathrm{i}\,0.35$	$-0.66 - \mathrm{i}\,0.56$
A, nb$^{1/2}$(anom.)	$0.13 + \mathrm{i}\,0.72$	$-0.19 + \mathrm{i}\,0.76$
A, nb$^{1/2}$(total)	$-0.57 + \mathrm{i}\,1.07$	$-0.85 + \mathrm{i}\,0.20$
(IV) Model-independent		
A, nb$^{1/2}$	-0.73 ± 0.17	$-0.78^{+0.08}_{-0.15}$
	$+\mathrm{i}\,(0.18 \pm 0.80)$	$+\mathrm{i}\,(0.32^{+0.09}_{-0.32})$

the total uncertainty about the non-resonant amplitude A_P and a strong correlation between A_P and resulting cross section values. A χ^2 value obtained for this fit is practically the same as for the above models, thus allowing to draw a conclusion on the consistency of the assumption about constant A_p with the experimental data.

5 Discussion

As it was already noted in the previous section, the results of the analysis of experimental data reveal a strong model dependence of the fitted values for cross sections and decay probabilities of ϕ meson. Thus it can be useful to compare other values obtained from these models. One particular thing in which the models differ is the description of the non-resonant amplitude.

For comparison, in each model we calculate the value of the non-resonant amplitude in the maximum of ϕ meson. This amplitude includes both the true non-resonant amplitude (B_P term), and the tails of ρ and ω mesons. The phase of the resonant term was fixed at $\varphi_\phi = 180^\circ$ to bring the amplitude for each model to the form similar to (17). For VDM and the anomalous contribution the non-resonant amplitude is then represented as

$$A_P = \left[\mathrm{i}\sqrt{4\pi\alpha^2} B_P - \sum_{V=\rho,\omega} A_V \right] e^{-\mathrm{i}\varphi_\phi}, \tag{18}$$

where $B_P \equiv 0$ for VDM as before. For the model-independent approach the amplitude A_P was used as obtained directly from the fit.

Obtained amplitudes are shown in the table 6. For the anomaly model the contribution from the ρ and ω mesons and anomalies are displayed separately, together with their sum. For the model-independent approach the results displayed are the same as in the table 5. A comparison of the amplitudes from models (I-III) with the model-independent approach (IV) reveals no obvious discrepancies in the values of this non-resonant term. The values of χ^2 (table 5) also look favorable for all models. Thus we conclude that the collected statistics in not sensitive enough to be able to discriminate between models or to determine exactly model parameters. However, the difference between amplitudes observed for the different models (table 6) at the level of one standard deviation may indicate that larger statistics can disambiguate the situation.

Despite the recent progress in the understanding of the anomalous contribution [5] there still remains a sort of ambiguity in its description, related also to the uncertainty in the parameterization of resonances' shapes. Due to this we consider our results obtained for the anomaly model as an indication of the necessity of further studies. Instead we prefer to draw the final result for VDM model, because until now there is no any strong evidence against VDM observed in e^+e^- data.

Table 7: Comparison of the observed decay probabilities with other recent measurements.

Experiment	Final state	$\mathrm{Br}(\phi \to \eta\gamma)$, %
This study	3γ	1.338 ± 0.053
PDG '98 [17]	**avg.**	1.26 ± 0.06
SND '98 [11]	7γ	1.246 ± 0.062
CMD-2 '95 [10]	$\pi^+\pi^-3\gamma$	1.18 ± 0.11
ND '84 [9]	3γ	1.30 ± 0.06
ND '84 [9]	7γ	1.4 ± 0.2
OLYA '83 [19]	3γ	0.88 ± 0.20
Andrews *et al.* '77 [20]	3γ	1.35 ± 0.29
ORSAY '76 [21]	3γ	1.5 ± 0.4
		$\mathrm{Br}(\phi \to \pi^0\gamma)$, 10^{-3}
This study	3γ	1.23 ± 0.10
ND '84 [9]	3γ	1.30 ± 0.13
ORSAY '76 [21]	3γ	1.4 ± 0.5

This also allows to compare these results directly with the results obtained earlier for the same model [9]. From (11,12) and (13–15) we obtain following values for the decay probabilities:

$$\mathrm{Br}(\phi \to \eta\gamma) = (1.338 \pm 0.012 \pm 0.052)\%, \quad (19)$$

$$\mathrm{Br}(\phi \to \pi^0\gamma) = (1.226 \pm 0.036^{+0.096}_{-0.089}) \times 10^{-3}, \quad (20)$$

where the systematic uncertainties include the errors quoted in (11,12) and uncertainties of the values $\mathrm{Br}(\phi \to e^+e^-)$ and $\mathrm{Br}(P \to \gamma\gamma)$ (13–15). Partial widths of the decays include also uncertainties from the Γ_ϕ determination, and are equal to

$$\Gamma(\phi \to \eta\gamma) = (58.9 \pm 0.5 \pm 2.4)\,\mathrm{keV}, \quad (21)$$

$$\Gamma(\phi \to \pi^0\gamma) = (5.40 \pm 0.16^{+0.43}_{-0.40})\,\mathrm{keV}. \quad (22)$$

In the determination of the partial widths of decays $\phi \to \eta\gamma$ and $\phi \to \pi^0\gamma$ some of the systematic effects are common to both, hence in their ratio the errors caused by these effects cancel:

$$\frac{\Gamma(\phi \to \eta\gamma)}{\Gamma(\phi \to \pi^0\gamma)} = 10.9 \pm 0.3^{+0.7}_{-0.8}. \quad (23)$$

The uncertainty of the last result is still determined by the systematic effects, where the main contribution comes from the uncertainty in the ϕ meson phase in the process (2).

From the results of the work [11], which studied the cross section of the process $e^+e^- \to \phi \to \eta\gamma \to 3\pi^0\gamma$ using the same experimental data sets, we can determine also the ratio of the partial widths for the decays $\eta \to 3\pi^0$ and $\eta \to \gamma\gamma$

$$\frac{\Gamma(\eta \to 3\pi^0)}{\Gamma(\eta \to \gamma\gamma)} = 0.796 \pm 0.016 \pm 0.016, \quad (24)$$

which is 1.1 standard deviation lower than the table value 0.821 ± 0.007 [17].

In table 7 we give a comparison of our results for the decay probabilities with all previous measurements. Our measurements are close to the world average values (marked PDG in the table) and individual measurements. It is worth mentioning here that practically all cited analyses are based on some modification of a simple VDM approach. Hence all results of previous measurements are subjected to the model dependence discussed above, although it is significant only for the most precise measurements.

6 Conclusion

The main results of these studies were presented in the eqs. (11), (12), (19-24). These results have a high statistical accuracy. Nevertheless, the precise determination of the decay parameters cannot

be achieved without the essential reduction of the systematic errors and better understanding of model dependence. In this respect the important is the question of the detailed study of the non-resonant amplitude in the resonance region, both experimental and theoretical. In the experimental study the improvement can be achieved with the precise study of the non-resonant region between ω and ϕ, and above ϕ meson. Further increase in the experimental statistics in the resonance region, especially at the slopes and tails of the resonance, will also help in understanding of the interference pattern of non-resonant and resonant terms. One more step in this direction could be the further analysis of the full statistic collected in the experiments SND and CMD-2, and the simultaneous analysis of different final states.

References

[1] L. Landsberg, Phys. Rep. **128**, 301 (1985).

[2] P. O'Donnel, Rev. Mod. Phys. **53**, 673 (1981).

[3] H. O'Connel *et al.*, Prog. Part. Nucl. Phys. **39**, 201 (1997).

[4] A. Bramon, A. Grau, and G. Pancheri, Phys. Lett. B **344**, 240 (1995).

[5] M. Benayoun *et al.*, Z. Phys. C **72**, 221 (1996).

[6] N. Achasov *et al.*, Int. Jour. of Mod. Phys. A **7**, 3187 (1992).

[7] E. Anashkin *et al.*, ICFA Instr. Bull. **5**, 18 (1988).

[8] V. Aulchenko *et al.*, in *Proceedings of the Workshop on Physics and Detectors for DAΦNE* (INFN, Frascati, 1991), p. 605.

[9] S. Dolinsky *et al.*, Phys. Rep. **202**, 99 (1991).

[10] R. Akhmetshin *et al.*, Phys. Lett. B **364**, 199 (1995).

[11] M. Achasov *et al.*, JETP Lett **68**, 573 (1998).

[12] M. Achasov *et al.*, Nucl. Instr. and Meth. A **411**, 337 (1998).

[13] M. Bekishev and V. Ivanchenko, Nucl. Instr. and Meth. A **361**, 138 (1995).

[14] E.A.Kurav and V.S.Fadin, Sov. J. Nucl. Phys. **41**, 466 (1985).

[15] A. Bukin *et al.*, in *MC91: Detector and Event Simulation in HEP* (NIKHEF-H, Amsterdam, 1991), pp. 79–85.

[16] B. Geshkenbein and M. Terentyev, Jour. of Nucl. Phys. **8**, 550 (1968).

[17] Particle Data Group, Eur. Phys. J. C **3**, (1998).

[18] R. Akhmetshin *et al.*, Phys. Lett. B **434**, 426 (1998).

[19] L. Kurdadze *et al.*, JETP Lett. **38**, 366 (1983).

[20] D. Andrews *et al.*, Phys. Rev. Lett. **38**, 198 (1977).

[21] G. Cosme *et al.*, Phys. Lett. B **63**, 352 (1976).